All-Digital Background Calibration Technique for Time-Interleaved ADC Using Pseudo Aliasing Signal

Junya Matsuno, Takafumi Yamaji, *Senior Member, IEEE*, Masanori Furuta, *Member, IEEE*, and Tetsuro Itakura, *Member, IEEE*

***Abstract*—A new digital background calibration technique for gain mismatches and sample-time mismatches in a Time-Interleaved Analog-to-Digital Converter (TI-ADC) is presented to reduce the circuit area. In the proposed technique, the gain mismatches and the sample-time mismatches are calibrated by using pseudo aliasing signals instead of using a bank of adaptive FIR filters which is conventionally utilized. The pseudo aliasing signals are generated and subtracted from an ADC output. A pseudo aliasing generator consists of the Hadamard transform and a fixed FIR filter. In case of a two-channel 10-bit TI-ADC, the proposed technique reduces the requirement for a word length of the FIR filter by about 50% without a look-up table (LUT) compared with the conventional technique. In addition, the proposed technique requires only one FIR filter compared with the bank of adaptive filters which requires (M-1) FIR filters in an M-channel TI-ADC.**

***Index Terms*—ADC, all-digital background calibration, derivative filter, fixed FIR, Hadamard transform, pseudo aliasing signal, time-interleaved.**

I. Introduction

TIME-INTERLEAVED Analog-to-Digital converters (TI-ADCs) [1] are widely used for high-speed data communication systems. A calibration technique is mostly required for TI-ADCs because of performance degradation due to gain mismatches and sample-time mismatches between individual channels [2], [3].

Analog and mixed signal calibration techniques have been used for the sample-time mismatch correction [4]–[7]. These techniques calibrate a delay of a clock path by adjusting a capacitance of varactors which are attached to outputs of clock buffers. An advantage of this technique is simplicity of its hardware elements. However, the analog correction technique limits an effective performance of the ADC due to process, supply voltage and temperature variations and a thermal noise.

An all-digital calibration technique is beneficial to eliminate issues of the analog and mixed-signal calibration. It has an advantages of the area reduction in an advanced process technology and it is unnecessary to re-design calibration circuits when the different process technology is applied.

Manuscript received September 18, 2012; revised December 29, 2012; accepted January 26, 2013. This paper was recommended by Associate Editor M.-D. Shieh.

J. Matsuno, M. Furuta and T. Itakura are with the Corporate Research and Development Center, Toshiba Corporation, Kawasaki 212-8582, Japan (e-mail: junya.matsuno@toshiba.co.jp).

T. Yamaji is with the Analog and Imaging IC Division, Toshiba Corporatoin Semiconductor and Storage Products Company, Kawasaki 212-8520, Japan.

Digital Object Identifier 10.1109/TCSI.2013.2249176

The all-digital calibration circuits can be divided in two blocks, a mismatch correction and an estimation. Conventionally, a bank of adaptive filters have been used as the mismatch correction block [8]–[13]. The sample-time mismatches are calibrated by adjusting the filter coefficients. However, this technique requires large amounts of area because the dynamic range of the filters which are in the main signal paths have to be equal to the dynamic range of the ADCs and the filter coefficients have to be calculated or stored in a LUT. In addition, (M-1) filters are required in a M-channel TI-ADC. A calibration technique using only one FIR fitler for small skew mismatch is presented in [15]. However, this technique also requires large dynamic range such as the technique using a bank of filters.

This paper presents an all-digital background calibration technique for the TI-ADC. The design challenge is reducing the circuit area. To reduce the circuit area, the mismatch correction technique using a pseudo aliasing signal is proposed. Since the gain mismatches and the sample-time mismatches result in residual aliasing signals [2], the pseudo aliasing signals are used to cancel the residual aliasing signals. The pseudo aliasing signals are generated from the ADC output by means of the Hadamard taransform and a fixed FIR filter with constant coefficients. The proposed technique reduces the calibration circuit area by three reasons: (1) only one FIR filter is required for the M-channel TI-ADC, (2) no coefficient calculator and no LUT are needed and (3) the dynamic range of the FIR filter is greatly reduced compered with the bank of adaptive filters.

The proposed technique also uses the pseudo aliasing signals in the mismatch estimation. In cases of a two-channel TI-ADC, the proposed technique is similar to the previously reported technique [8] and [12]. However, in a M-channel TI-ADC where M is an integer more than two, the proposed technique achieves the smaller circuit area and a shorter convergence time by expanding the Hadamard matrix compared with the conventional technique [12] which uses the chopper for symmetrical channels similarly in [8].

The remainder of this paper is organized as follows. In Section II, the residual aliasing signal due to the gain mismatches and the sample-time mismatches in TI-ADC is reviewed. The proposed calibration technique using the pseudo aliasing signal is introduced in Section III. Section IV presents polyphase implementation of the proposed calibration. Simulation results are presented in Section V. Section VI concludes this paper.

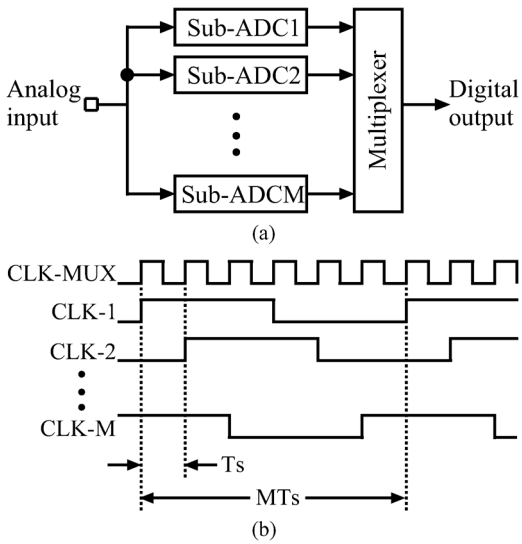

Fig. 1. M-channel Time-Interleaved ADC. (a) Block diagram; (b) timing diagram.

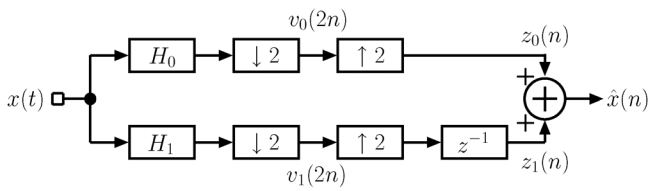

Fig. 2. Block diagram of two-channel TI-ADC.

II. Residual Aliasing Due to Gain and Sample-Time Mismatches

A block diagram and a timing diagram of the M-channel TI-ADC are shown in Fig. 1. Each channel consists of a sub-ADC, where each channel has the same sampling period of MT_s but the difference between the sampling times of the neighboring channels is T_s. An analog input signal is sequentially sampled and digitized by the sub-ADCs of the individual channels to produce digital streams, and the digital streams from the M-channels are then multiplexed to generate a final ADC digital output signal. The ADC equivalent sampling period is T_s.

Fig. 2 shows a block diagram of the two-channel time-interleaved ADC. For simplicity, we consider a two-channel model without a quantization noise. $H_k(j\omega)$ $(k = 0, 1)$ are channel frequency responses, here $-\pi < \omega \leq \pi$. The delay function is $z^{-1} = e^{-j\omega}$. A sum of a mismatch of each channel is equal to zero because the mismatches are defined as the difference from the average.

$H_0(j\omega)$ and $H_1(j\omega)$ have gain mismatches and sample-time mismatches. These channel responses are written as

$$\begin{aligned} H_0(j\omega) &= (1+\Delta_{g0})e^{j\omega\Delta_{t0}} \\ H_1(j\omega) &= (1+\Delta_{g1})e^{j\omega(1+\Delta_{t1})} \end{aligned} \tag{1}$$

where Δ_{gk} is the gain mismatch and Δ_{tk} is the sample-time mismatch in k-th channel and $(\Delta_{g0}+\Delta_{g1}) = (\Delta_{t0}+\Delta_{t1}) = 0$.

The discrete Fourier transform (DFT) of downsampled signals $v_k(2n)$ are

$$\begin{bmatrix} V_0(j2\omega) \\ V_1(j2\omega) \end{bmatrix} = \frac{1}{2} \begin{bmatrix} H_0(j\omega) & H_0\left(j(\omega-\pi)\right) \\ H_1(j\omega) & H_1\left(j(\omega-\pi)\right) \end{bmatrix} \begin{bmatrix} X(j\omega) \\ X\left(j(\omega-\pi)\right) \end{bmatrix} \tag{2}$$

where $X(j\omega)$ is the DFT of a sampling sequence $x(n)$ of an analog signal $x(t)$ as shown in Fig. 3(a) and $X(j(\omega-\pi))$ is an aliasing signal. The DFT of a reconstructed signal $\hat{x}(n)$ is

$$\begin{aligned} \hat{X}(j\omega) &= Z_0(j\omega) + Z_1(j\omega) = V_0(j2\omega) + e^{-j\omega}V_1(j2\omega) \\ &= \frac{1}{2}\left\{(1+\Delta_{g0})e^{j\omega\Delta_{t0}} + (1+\Delta_{g1})e^{j\omega\Delta_{t1}}\right\} X(j\omega) \\ &\quad + \frac{1}{2}\left\{(1+\Delta_{g0})e^{j(\omega-\pi)\Delta_{t0}} - (1+\Delta_{g1})e^{j(\omega-\pi)\Delta_{t1}}\right\} \\ &\quad \times X\left(j(\omega-\pi)\right) \end{aligned} \tag{3}$$

where $Z_k(j\omega)$ $(k = 0, 1)$ is an output signal of the individual channels. When $\Delta_{g0} = \Delta_{g1}$ and $\Delta_{t0} = \Delta_{t1}$, the aliasing signal is perfectly canceled because the aliasing signal of $Z_0(j\omega)$ and $Z_1(j\omega)$ has a same power and a reversed phase as shown in Fig. 3(b), (c). However, since $\Delta_{g0} \neq \Delta_{g1}$ and $\Delta_{t0} \neq \Delta_{t1}$, the aliasing signal remains and degrades effective resolution of the ADC as shown in Fig. 3(d). Assuming that Δ_{gk} and Δ_{tk} are much less than 1 in an actual TI-ADC, (3) is simplified to

$$\begin{aligned} \hat{X}(j\omega) \approx X(j\omega) + \frac{1}{2}\{&(\Delta_{g0}-\Delta_{g1}) \\ &+ j(\omega-\pi)(\Delta_{t0}-\Delta_{t1})\} X\left(j(\omega-\pi)\right) \end{aligned} \tag{4}$$

where the second term and the third term show residual aliasing signals due to the gain mismatch and the sample-time mismatch, respectively. $j(\omega-\pi)$ implies that a residual aliasing due to the sample-time mismatch have a function of a derivative. A compensated signal can be obtained by cancelling the second term and the third term.

III. Proposed Calibration Technique

Fig. 4 shows a block diagram of the proposed calibration architecture overview in the two-channel TI-ADC. The key idea is using the pseudo aliasing signal instead of using the bank of adaptive filter for hardware reduction of correction circuits. The pseudo aliasing signal $\hat{x}_e(n)$ generated by a pseudo aliasing generator have same frequency element as the residual aliasing signal. The residual aliasing signal is cancelled by subtracting the pseudo aliasing signal $\hat{x}_e(n)$ with a suitable coefficient α which is produced by the mismatch estimation block. The residual aliasing signal has less signal dynamic range compared with the desired signal. The reduction of the signal word length for the pseudo aliasing generator achieves the hardware minimization of the correction circuit.

A. Pseudo Aliasing Generator

Fig. 5 shows a conceptual view of the pseudo aliasing generator in the two-channel TI-ADC. An orthogonal transform enables a separation of the desired signal and the aliasing one. Especially, the Hadamard transform is the best choice for the minimum hardware implementation. The pseudo aliasing signal $\hat{X}_e(j\omega)$ is obtained by subtracting the output of one channel

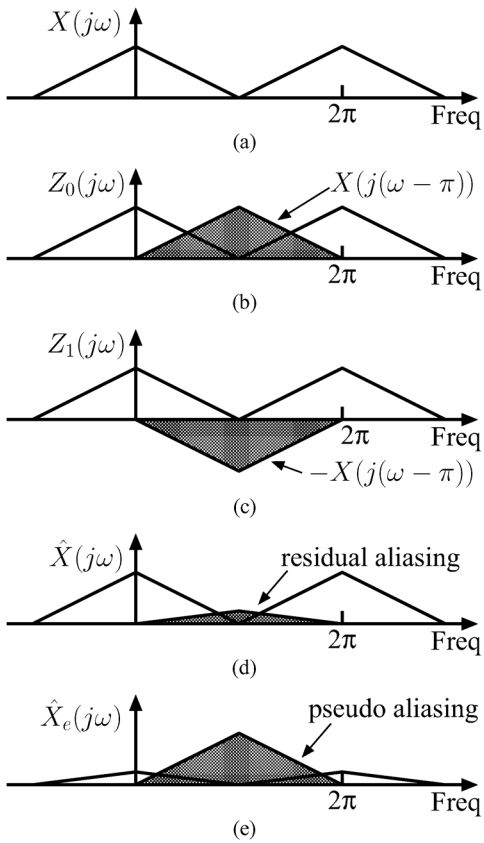

Fig. 3. Spectrum of $x(n)$, $z_0(n)$, $z_1(n)$, $\hat{x}(n)$ and $\hat{x}_e(n)$. (a) Spectrum of $x(n)$; (b) spectrum of $z_0(n)$; (c) spectrum of $z_1(n)$; (d) spectrum of $\hat{x}(n)$; (e) spectrum of $\hat{x}_e(n)$.

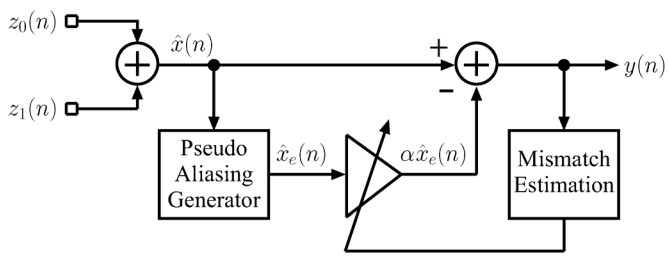

Fig. 4. Overview of the proposed architecture in two-channel TI-ADC.

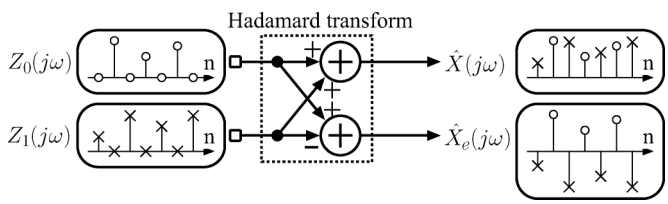

Fig. 5. Concept of pseudo aliasing generator.

from the output of the other channel. The spectrum of the reconstructed signal $\hat{X}(j\omega)$ and the pseudo aliasing signal $\hat{X}_e(j\omega)$ can be written as

$$\begin{bmatrix} \hat{X}(j\omega) \\ \hat{X}_e(j\omega) \end{bmatrix} = \boldsymbol{F} \begin{bmatrix} Z_0(j\omega) \\ Z_1(j\omega) \end{bmatrix}, \boldsymbol{F} = \begin{bmatrix} 1 & 1 \\ 1 & -1 \end{bmatrix} \tag{5}$$

where $\boldsymbol{F}$ is the Hadamard transform of order 2. The spectrum $\hat{X}_e(j\omega)$ of the pseudo aliasing signal $x_e(n)$ is shown in Fig. 3(e).

B. Subtraction of Aliasing

A compensated signal $Y(j\omega)$ can be derived by subtracting the pseudo aliasing signal $\hat{X}_e(j\omega)$, which are multiplied by the coefficient α, from reconstructed signal $\hat{X}(j\omega)$

$$\begin{aligned} Y(j\omega) &= \hat{X}(j\omega) - \alpha\hat{X}_e(j\omega) \\ &= \frac{1}{2}\left\{(1+\Delta_{g0})e^{j\omega\Delta_{t0}} + (1+\Delta_{g1})e^{j\omega\Delta_{t1}}\right. \\ &\qquad - \alpha(1+\Delta_{g0})e^{j\omega\Delta_{t0}} \\ &\qquad \left. +\alpha(1+\Delta_{g1})e^{j\omega\Delta_{t1}}\right\} X(j\omega) \\ &\quad + \frac{1}{2}\left\{(1+\Delta_{g0})e^{j(\omega-\pi)\Delta_{t0}}\right. \\ &\qquad - (1+\Delta_{g1})e^{j(\omega-\pi)\Delta_{t1}} \\ &\qquad - \alpha(1+\Delta_{g0})e^{j(\omega-\pi)\Delta_{t0}} \\ &\qquad \left. -\alpha(1+\Delta_{g1})e^{j(\omega-\pi)\Delta_{t1}}\right\} \\ &\quad \times X\left(j(\omega-\pi)\right). \end{aligned} \tag{6}$$

We can calculate the coefficient α to cancel the aliasing signal $X(j(\omega-\pi))$,

$$\begin{aligned} &(1+\Delta_{g0})e^{j(\omega-\pi)\Delta_{t0}} - (1+\Delta_{g1})e^{j(\omega-\pi)\Delta_{t1}} \\ &\quad -\alpha(1+\Delta_{g0})e^{j(\omega-\pi)\Delta_{t0}} - \alpha(1+\Delta_{g1})e^{j(\omega-\pi)\Delta_{t1}} = 0 \\ &\Rightarrow \alpha = -\frac{(1+\Delta_{g0})e^{j(\omega-\pi)\Delta_{t0}} - (1+\Delta_{g1})e^{j(\omega-\pi)\Delta_{t1}}}{(1+\Delta_{g0})e^{j(\omega-\pi)\Delta_{t0}} + (1+\Delta_{g1})e^{j(\omega-\pi)\Delta_{t1}}}. \end{aligned} \tag{7}$$

The residual aliasing signal is removed from the reconstruction signal when the coefficient α converges on the value of (7). Assuming that Δ_{gk} and Δ_{tk} ($k = 0, 1$) are much less than 1 in the actual TI-ADC, (7) and $\hat{X}_e(j\omega)$ are simplified to

$$\begin{aligned} \alpha &\approx \frac{1}{2}\left\{(\Delta_{g0}-\Delta_{g1}) + j(\omega-\pi)(\Delta_{t0}-\Delta_{t1})\right\}, \\ \hat{X}_e(j\omega) &\approx X\left(j(\omega-\pi)\right). \end{aligned} \tag{8}$$

We can see that $\alpha\hat{X}_e(j\omega)$ in (8) is equal to the second and third term in (4). $j(\omega-\pi)$ implies that the proposed calibration technique needs a fixed FIR filter which produce a derivative of the pseudo aliasing signal. $\alpha\hat{X}_e(j\omega)$ can be rewritten as

$$\begin{aligned} \alpha\hat{X}_e(j\omega) &\approx \frac{1}{2}\left\{(\Delta_{g0}-\Delta_{g1}) + j(\omega-\pi)(\Delta_{t0}-\Delta_{t1})\right\}\hat{X}_e(j\omega) \\ &= \frac{1}{2}(\Delta_{g0}-\Delta_{g1})\hat{X}_e(j\omega) + \frac{1}{2}(\Delta_{t0}-\Delta_{t1})\hat{X}'_e(j\omega) \\ &= \omega_{g1}\hat{X}_e(j\omega) + \omega_{t1}\hat{X}'_e(j\omega) \end{aligned} \tag{9}$$

where

$$\hat{X}'_e(j\omega) = j(\omega-\pi)\hat{X}_e(j\omega)$$

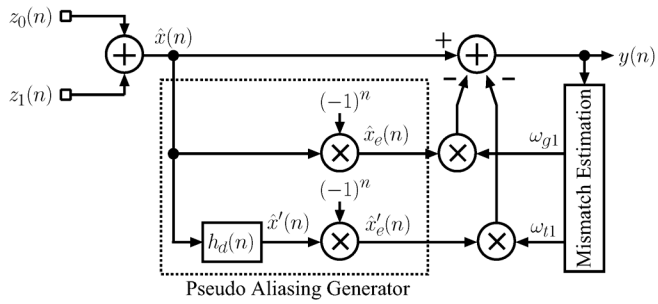

Fig. 6. Proposed structure in two-channel TI-ADC.

$$\omega_{g1} = \frac{(\Delta_{g0} - \Delta_{g1})}{2}$$
$$\omega_{t1} = \frac{(\Delta_{t0} - \Delta_{t1})}{2} \tag{10}$$

respectively. $\omega_{g1}\hat{X}_e(j\omega)$ and $\omega_{t1}\hat{X}'_e(j\omega)$ in (9) show the pseudo aliasing signal due to the gain mismatch and the sample-time mismatch.

Fig. 6 shows the actual implementation of the proposed calibration technique based on (9). The relation between $\hat{x}(n)$ and $\hat{x}_e(n)$ which are obtained by Hadamard transform can be written as $\hat{x}_e(n) = (-1)^n\hat{x}(n)$ as shown in Fig. 5. An ideal discrete-time derivative filter in Fig. 6 has the transfer function $H_d(j\omega) = j\omega$ by multiplication $(-1)^n$ for the derivation $j(\omega - \pi)$. The impulse response of the derivative filter is

$$h_d(n) = \begin{cases} \frac{cos(n\pi)}{n} & (n \neq 0) \\ 0. & (n = 0) \end{cases} \tag{11}$$

The filter coefficients are determined by multiplying the exact coefficients by a window function such as the Hanning window to reduce the influence of a truncation error. The weights ω_{g1} and ω_{t1} are generated by the mismatch estimation block.

The proposed calibration technique requires no coefficient calculator and no LUT because the derivative filter in (11) has constant coefficients compared with the conventional technique which requires the calculator or the LUT to produce the coefficients of the adaptive FIR filter. The calculator and the LUT require large hardware due to long word length for wide dynamic range and fine resolution of the sample-time mismatch.

C. Dynamic Range of the Calibration Circuit

The proposed technique using the pseudo aliasing signal instead of the bank of adaptive filter can greatly reduce the hardware of the mismatch correction circuit. The aliasing signal for cancelling the residual aliasing signal has less signal dynamic range compared with the dynamic range of the conventional adaptive FIR filter which have to be equal to the dynamic range of the ADC because the filter are in the main signal path. The reduction of the signal word length for the pseudo aliasing generator achieves the hardware minimization of the correction circuit.

We can calculate the ratio of the dynamic range between the reconstruction signal $\hat{X}(j\omega)$ and the pseudo aliasing signal $\hat{X}_e(j\omega)$ with α when the gain mismatches are equal to zero and Δ_{tk} $(k = 0, 1)$ are much less than 1,

$$\left|\frac{\alpha\hat{X}_e(j\omega)}{\hat{X}(j\omega)}\right| \approx |\alpha| = \frac{1}{2}(\Delta_{t0} - \Delta_{t1})|\omega - \pi| \tag{12}$$

where the dynamic range of the reconstruction signal $\hat{X}(j\omega)$ and the pseudo aliasing signal $\hat{X}_e(j\omega)$ are approximately equal $|\hat{X}(j\omega)| \approx |\hat{X}_e(j\omega)|$. The pseudo aliasing generator with the fixed FIR filter is essential to the successful implementation in a small area because the dynamic range of the pseudo aliasing signal with α is much less than the reconstruction signal. For example, the dynamic range of the pseudo aliasing signal with α is $20\log_{10}(|(\omega - \pi)(\Delta_{t0} - \Delta_{t1})/2|) = -36.1$ dB where the sample-time mismatch $(\Delta_{t0} - \Delta_{t1}) = 0.01$ and the frequency $\omega = 0$ for a maximum value in (12). The signal word length of the fixed FIR filter can be reduced about 5.0 bits compared with the conventional adaptive filter. The signal word length of the calibration circuit for the gain mismatch can also be reduced,

$$\left|\frac{\alpha\hat{X}_e(j\omega)}{\hat{X}(j\omega)}\right| \approx \frac{1}{2}(\Delta_{g0} - \Delta_{g1}). \tag{13}$$

The dynamic range of the pseudo aliasing signal with α is $20\log_{10}((\Delta_{g0} - \Delta_{g1})/2) = -46.0$ dB which can be reduced about 7.0 bits where the gain mismatch $(\Delta_{g0} - \Delta_{g1}) = 0.01$.

D. Proposed Technique in M-Channel TI-ADC

The proposed circuit adapts to a variety of channels by expanding the Hadamard matrix. Even in the M-channel TI-ADC case, the derivation for $\hat{x}(n)$ requires only one FIR filter compared with the conventional technique which require $(M - 1)$ FIR filters [8]. The proposed technique has a major advantage for reduction of the calibration hardware of the TI-ADC in many channels. Fig. 7 shows the proposed structure in a four-channel TI-ADC. T_1, T_2 and T_3 in Fig. 7 are

$$T_1 = \begin{cases} 1, & (n = 4i) \\ -1 & (n = 4i + 1) \\ 1, & (n = 4i + 2) \\ -1 & (n = 4i + 3) \end{cases} T_2 = \begin{cases} 1, & (n = 4i) \\ 1, & (n = 4i + 1) \\ -1 & (n = 4i + 2) \\ -1 & (n = 4i + 3) \end{cases}$$
$$T_3 = \begin{cases} 1, & (n = 4i) \\ -1 & (n = 4i + 1) \\ -1 & (n = 4i + 2) \\ 1, & (n = 4i + 3) \end{cases} \tag{14}$$

where i is an arbitrary integer. T_1, T_2 and T_3 are row vectors in the Hadamard transform expect for a row vector $T_0 = (1, 1, 1, 1)$ because the sum of the mismatch in each channel is equal to zero as described in Section II.

We consider the M-channel model without a quantization noise. The channel frequency responses in (1) are rewritten as

$$H_k(j\omega) = (1 + \Delta_{gk})e^{j\omega(k + \Delta_{tk})} \tag{15}$$

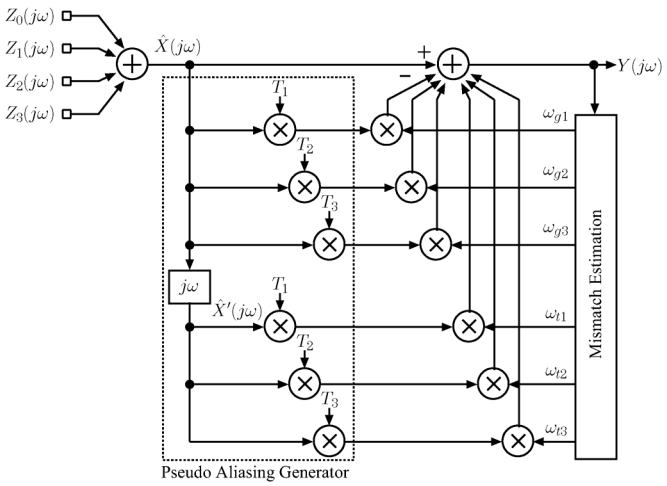

Fig. 7. Proposed structure in four-channel TI-ADC.

where $k = 0, \ldots, M-1$. The DFT of the downsampled signal in (2) are rewritten as

$$V_k(jM\omega) = \frac{1}{M}\sum_{i=0}^{M-1} H_k\left(j\left(\omega - \frac{2\pi i}{M}\right)\right) X\left(j\left(\omega - \frac{2\pi i}{M}\right)\right). \tag{16}$$

The DFT of the reconstructed signal in (3) is rewritten as

$$\hat{X}(j\omega) = \sum_{k=0}^{M-1} Z_k(j\omega) = \sum_{k=0}^{M-1} e^{-jk\omega} V_k(jM\omega). \tag{17}$$

The spectrum of the reconstructed signal and the pseudo aliasing signals in the M-channel TI-ADC can be written as

$$\begin{bmatrix} \hat{X}(j\omega) \\ \hat{X}_{e1}(j\omega) \\ \vdots \\ \hat{X}_{e(M-1)}(j\omega) \end{bmatrix} = \boldsymbol{F} \begin{bmatrix} Z_0(j\omega) \\ Z_1(j\omega) \\ \vdots \\ Z_{M-1}(j\omega) \end{bmatrix} \tag{18}$$

where $\boldsymbol{F}$ is the Hadamard transform of order M. The derived signals in (18) can be obtained as

$$\begin{bmatrix} \hat{X}'(j\omega) \\ \hat{X}'_{e1}(j\omega) \\ \vdots \\ \hat{X}'_{e(M-1)}(j\omega) \end{bmatrix} = \boldsymbol{F} \begin{bmatrix} Z'_0(j\omega) \\ Z'_1(j\omega) \\ \vdots \\ Z'_{M-1}(j\omega) \end{bmatrix} \tag{19}$$

where,

$$Z'_k(j\omega) = \frac{1}{M} e^{-jk\omega} \sum_{i=0}^{M-1} e^{jk\left(\omega - \frac{2\pi i}{M}\right)} \times j\left(\omega - \frac{2\pi i}{M}\right) \hat{X}\left(j\left(\omega - \frac{2\pi i}{M}\right)\right). \tag{20}$$

The compensated signal is written as

$$Y(j\omega) = \hat{X}(j\omega) - \sum_{i=1}^{M-1} w_{gi}\hat{X}_{ei}(j\omega) - \sum_{i=1}^{M-1} w_{ti}\hat{X}'_{ei}(j\omega). \tag{21}$$

We can calculate the coefficients w_{gi} and w_{ti} to cancel the residual aliasing signals when the Δ_{gk} and Δ_{tk} $(k = 0, \ldots, M-1)$ are much less than 1

$$\begin{bmatrix} w_{g0} \\ w_{g1} \\ \vdots \\ w_{g(M-1)} \end{bmatrix} \approx \frac{1}{M}\boldsymbol{F} \begin{bmatrix} \Delta_{g0} \\ \Delta_{g1} \\ \vdots \\ \Delta_{g(M-1)} \end{bmatrix} \tag{22}$$

$$\begin{bmatrix} w_{t0} \\ w_{t1} \\ \vdots \\ w_{t(M-1)} \end{bmatrix} \approx \frac{1}{M}\boldsymbol{F} \begin{bmatrix} \Delta_{t0} \\ \Delta_{t1} \\ \vdots \\ \Delta_{t(M-1)} \end{bmatrix} \tag{23}$$

where $\omega_{g0} = \omega_{t0} = 0$ because the sum of the mismatch in each channel is equal to zero as described in Section II. For example, the coefficients in the four-channel TI-ADC as shown in Fig. 7 are

$$\begin{aligned} \omega_{g1} &= \frac{1}{4}(\Delta_{g0} - \Delta_{g1} + \Delta_{g2} - \Delta_{g3}) \\ \omega_{g2} &= \frac{1}{4}(\Delta_{g0} + \Delta_{g1} - \Delta_{g2} - \Delta_{g3}) \\ \omega_{g3} &= \frac{1}{4}(\Delta_{g0} - \Delta_{g1} - \Delta_{g2} + \Delta_{g3}) \\ \omega_{t1} &= \frac{1}{4}(\Delta_{t0} - \Delta_{t1} + \Delta_{t2} - \Delta_{t3}) \\ \omega_{t2} &= \frac{1}{4}(\Delta_{t0} + \Delta_{t1} - \Delta_{t2} - \Delta_{t3}) \\ \omega_{t3} &= \frac{1}{4}(\Delta_{t0} - \Delta_{t1} - \Delta_{t2} + \Delta_{t3}). \end{aligned} \tag{24}$$

E. Mismatch Estimation

The proposed technique also uses the pseudo aliasing signals generated by Hadamard transform and the FIR filter in the mismatch estimation. In cases of the two-channel TI-ADC, the proposed technique is similar to the previously reported techniques [8] and [12] which use a chopper and the FIR filter because the a row vector $(1, -1)$ in the Hadamard transform of order 2 is identical to the function of the chopper.

Our estimation technique requires only one FIR filter for the M-channel estimation in a similar way to the Section III-D compared with [12] which requires M FIR filters. This reduces the circuit area for the proposed technique. In addition, our estimation technique can simultaneously converge for each channel compared with the convergence time in [12] which increases in proportion to the number of channels because the convergence for each symmetrical channels have to be staggered in series.

Fig. 8 shows the mismatch estimation in the M-channel TI-ADC. The mismatch estimation block consists of the pseudo aliasing generator, correlators and a notch filter. There are a few limitations in common with [8]. The notch filter produces nulls at $k\pi/M$ to avoid the estimation error, where $k = 1, \ldots, M-1$. As described in Section III-A, the pseudo aliasing generator generates pseudo aliasing signals $y_{ek}(n)$ and $y'_{ek}(n)$ which is the derived signal of $y_{ek}(n)$. Fig. 9 shows a block diagram of a correlator. The correlations are calculated between the output signal of the notch filter $y_n(n)$ and the pseudo aliasing signals

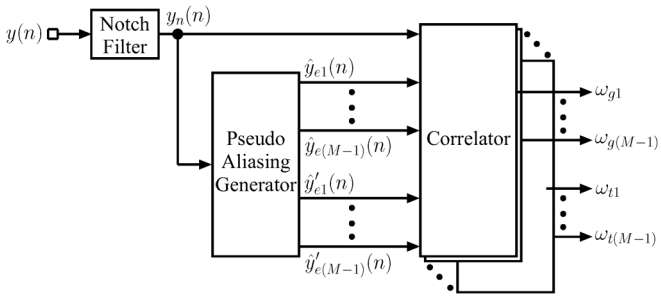

Fig. 8. Mismatch estimation in M-channel TI-ADC.

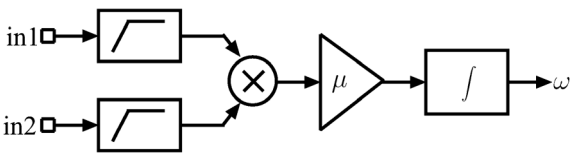

Fig. 9. Correlator.

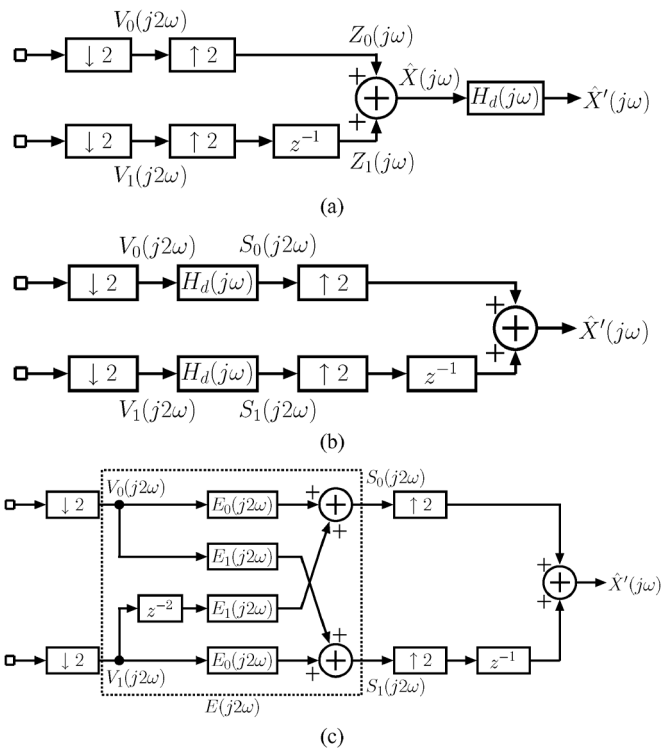

Fig. 10. Polyphase implementation of the derivative filter $H_d(j\omega)$ for two-channel TI-ADC. (a) Normal implementation; (b) split implementation; (c) polyphase implementation with cross-coupled structure.

$y_{ek}(n)$ and $y'_{ek}(n)$. The DC values of the input signals have to be eliminated by the DC offset canceller because the correlation of these DC values make a estimation inaccurate. As long as the compensated signal has the residual aliasing signal, a feedback makes the correlation close to zero. The coefficients of (22) and (23) can be derived from an updating of the correlation by an adaptive correlation algorithm

$$w_{gk}(n+1) = w_{gk}(n) + \mu_{gk}\left(y_n(n)\hat{y}_{ek}(n)\right) \quad (25)$$

$$w_{tk}(n+1) = w_{tk}(n) + \mu_{tk}\left(y_n(n)\hat{y}'_{ek}(n)\right) \quad (26)$$

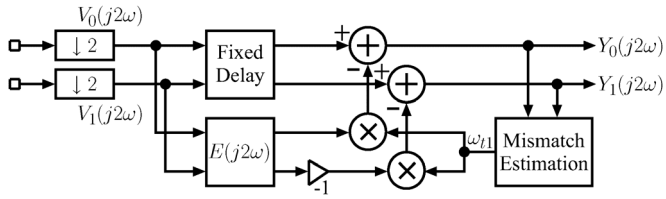

Fig. 11. Polyphase structure of the proposed calibration for sample-time mismatch in two-channel ADC.

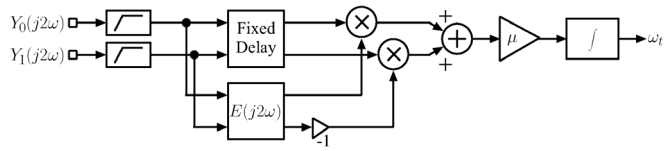

Fig. 12. Polyphase structure of the misamtch estimation block for sample-time mismatch in two-channel ADC.

where $k = 1, \ldots, M-1$, μ_{gk} and μ_{tk} are the adaptation step sizes for w_{gk} and w_{tk}.

IV. Polyphase Implementation

The calibration should be implemented just after the sub ADCs when the sampling period T_s is less than the usable period of a logic synthesis tool. This calibration can be realized by a polyphase transform. Fig. 10 shows a polyphase implementation of the derivative filter $H_d(j\omega)$ for the two-channel TI-ADC. The equivalent output signal $\hat{X}'(j\omega)$ can be obtained from the Fig. 10(a)–(c). Let $H_d(j\omega) = \sum_{n=-\infty}^{\infty} h_d(n)e^{-j\omega n}$ be a transfer function representing a filter. We can re-express in the form

$$\begin{aligned} H_d(j\omega) &= E_0(j2\omega) + e^{-j\omega}E_1(j2\omega) \\ E_0(j2\omega) &= \sum_{n=-\infty}^{\infty} h_d(2n)e^{-j2\omega n} \\ E_1(j2\omega) &= \sum_{n=-\infty}^{\infty} h_d(2n+1)e^{-j2\omega n}. \end{aligned} \quad (27)$$

The implementation of the function $e^{-j\omega}$ at the output of the sub ADCs which are downsampled signals is realized by a cross-coupled structure

$$\begin{aligned} e^{-j\omega}V_0(j2\omega) &= \mathcal{F}\left[v_0(2n-1)\right] = \mathcal{F}\left[x(2n-1)\right] \\ &= \mathcal{F}\left[v_1(2n-2)\right] = e^{-j2\omega}V_1(j2\omega) \quad (28) \\ e^{-j\omega}V_1(j2\omega) &= \mathcal{F}\left[v_1(2n-1)\right] = \mathcal{F}\left[x(2n)\right] \\ &= \mathcal{F}\left[v_0(2n)\right] = V_0(j2\omega) \quad (29) \end{aligned}$$

where

$$\begin{aligned} v_0(2n) &= x(2n) \\ v_1(2n) &= x(2n+1) \end{aligned} \quad (30)$$

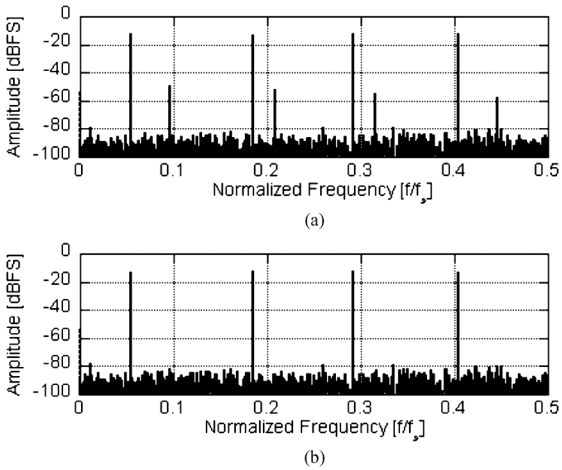

Fig. 13. Spectrum of output of two-channel TI-ADC with/without calibration. (a) Output spectrum without correction; (b) output spectrum with correction.

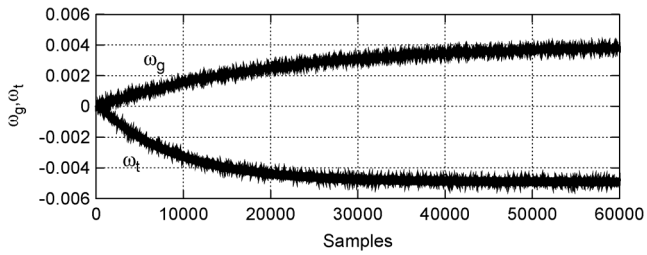

Fig. 14. Convergence of correlation output in two-channel TI-ADC.

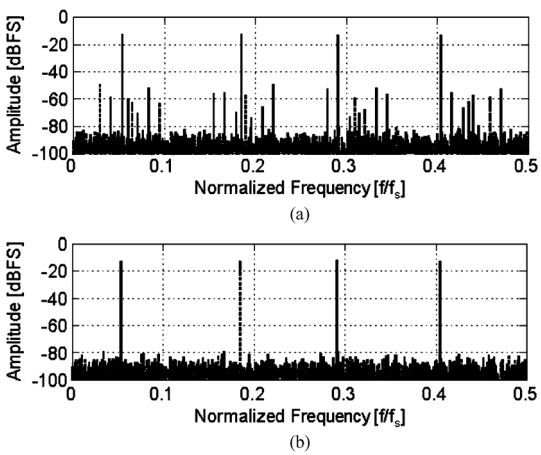

Fig. 15. Spectrum of output of eight-channel TI-ADC with/without calibration in polyphase structure. (a) Output spectrum without correction; (b) output spectrum with correction.

and the gain mismatch and the sample-time mismatch are zero for simplicity. The output signal $S_k(j\omega)$ ($k = 0, 1$) of the filter in Fig. 10(b), (c) can be calculate as

$$\begin{aligned} S_0(j2\omega) &= V_0(j2\omega)H_d(j\omega) \\ &= V_0(j2\omega)\left\{E_0(j2\omega) + e^{-j\omega}E_1(j2\omega)\right\} \\ &= V_0(j2\omega)E_0(j2\omega) + e^{-j2\omega}V_1(j2\omega)E_1(j2\omega) \qquad (31) \\ S_1(j2\omega) &= V_1(j2\omega)H_d(j\omega) \\ &= V_1(j2\omega)E_0(j2\omega) + V_0(j2\omega)E_1(j2\omega). \qquad (32) \end{aligned}$$

A block diagram of the polyphase structure of the proposed calibration technique for the sample-time mismatch in the two-channel TI-ADC is shown in Fig. 11, where $E(j2\omega)$ is the same in the Fig. 10. Fig. 12 shows the polyphase structure of the mismatch estimation block for the sample-time mismatch in the two-channel TI-ADC. The polyphase implementation can adapt a variety of channels by expanding the Hadamard matrix.

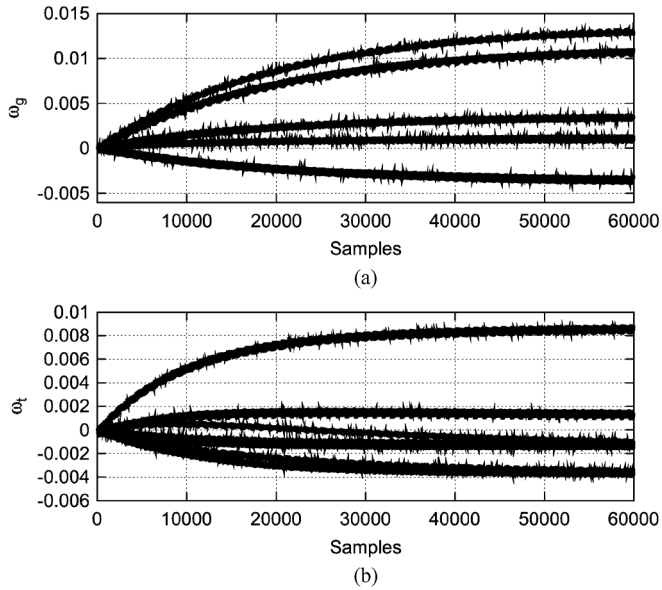

Fig. 16. Convergence of correlation output (a) w_g and (b) w_t in eight-channel TI-ADC.

V. Simulation

The proposed calibration technique was simulated for a 10 bit TI-ADC in a C language. In Simulations, a 31-tap fixed FIR filter is used to obtain the derivative function. The filter coefficients are determined by multiplying the exact coefficients by the Hanning window to reduce a truncation error.

Fig. 13 shows the output spectrum of the two-channel TI-ADC when input signal frequencies were $\omega_1 = 0.05f_s$, $\omega_2 = 0.18f_s$, $\omega_3 = 0.29f_s$, $\omega_4 = 0.405f_s$, respectively. The gain mismatch and the sample-time mismatch Δ_{g0}, Δ_{g1}, Δ_{t0}, Δ_{t1} were 0, -0.008, 0, 0.01, respectively. The adaptation step size are $\mu_g = \mu_t = 2^{-12}$. We choose the adaptation step sizes by using simulations to achieve reasonably fast convergence and small steady-state parameter variations [14]. In the compensated signal shown in Fig. 13(b), the aliasing signals due to mismatches are canceled out in contrast to the output signal without correction shown in Fig. 13(a). Fig. 14 shows the convergences of the correlation outputs. We can see that ω_g and ω_t finally converge at 0.004 and -0.005 as described in (10). Fig. 15 shows the output spectrum of the eight-channel TI-ADC in the polyphase structure with the gain mismatches and the sample-time mismatches. The gain mismatches and the sample-time mismatches Δ_{gk} and Δ_{tk} ($k = 0, \ldots, 7$) were 0, 0.01, 0.03, -0.01, 0.02, 0, -0.02, 0.04 and 0, 0.01, 0.02, 0, 0.03, 0.02, 0, 0.01, respectively. We can also see the compensated output shown in Fig. 15(b) in contrast to the output signal without correction as shown in Fig. 15(a). Fig. 16(a) and (b) shows the convergences of correlation outputs w_{gk} and w_{tk} ($k = 1, \ldots, 7$) for gain mismatches and sample-time mismatches. The convergence time in the eight-channel TI-ADC

TABLE I
HARDWARE COMPARISON

	ADC	Filter		
	dynamic range[bit]	Taps	Coefficients word length[bit]	Signal word length[bit]
Conventional	10	33	14	10
this work	10	31	13	**5**

	Additional blocks		
	LUT	adder	multiplier
Conventional	14b×33×4	nothing	nothing
this work	**nothing**	10b+12b	10b×6b

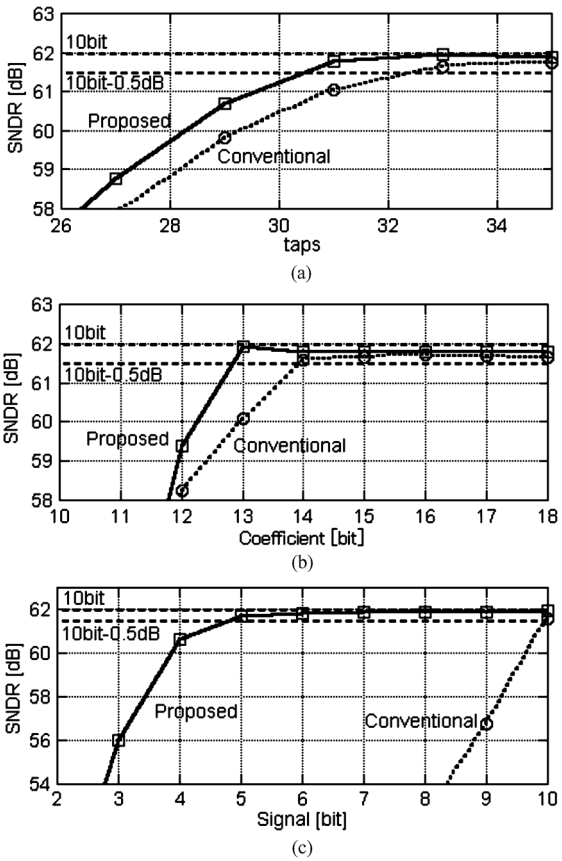

Fig. 17. SNDR versus parameters of filter. (a) SNDR versus filter taps; (b) SNDR versus coefficient word length; (c) SNDR versus signal word length.

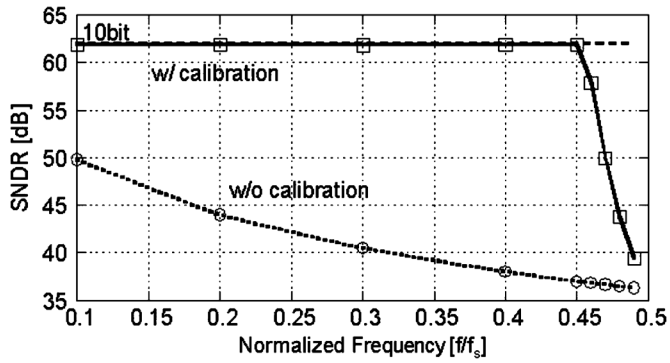

Fig. 18. SNDR versus input frequency with/without calibration.

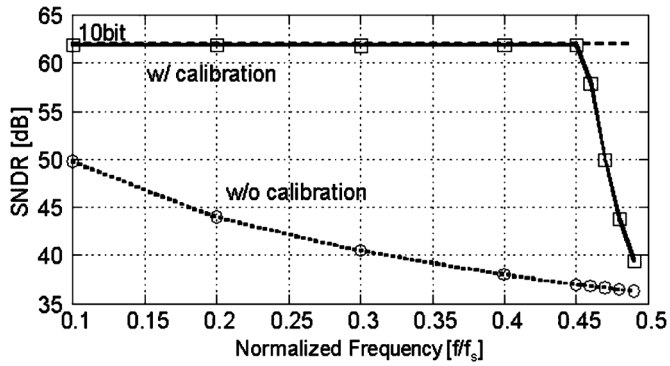

Fig. 19. SNDR versus sample-time mismatch with/without calibration.

in Fig. 16(b) is approximate equal to the convergence time in the two-channel TI-ADC in Fig. 14 for the sample-time mismatches compared with the convergence time in [12] which increase in proportion to the number of channels.

Next, we compare the hardware of the correction FIR filter for the sample-time mismatch with the conventional adaptive filter. The conventional and the proposed techniques utilize one filter for $\Delta_{tk} \ll 1$ ($k = 0, 1$) in the two-channel TI-ADC [8]. The hardware of the filter is compared based on 0.5 dB SNDR degradation for $\Delta_{g0} = \Delta_{g1} = \Delta_{t0} = 0$ and $\Delta_{t1} = 0.01$. The input signal is sinusoidal at $\omega = 0.45 f_s$, and the resolution of the ADC is 10 bits. Fig. 17 shows SNDR versus a number of filter taps, SNDR versus a coefficient word length and SNDR versus a signal word length, respectively. Table I shows the hardware comparison of the conventional and the proposed techniques for the timing mismatch. The requirements for the number taps and the coefficient word length are approximately equal. The proposed calibration technique can reduce the signal word length of the FIR filter by approximately 50% without LUT compared with the conventional technique. The additional latencies due to additional multipliers and adders have little effect on the sampling speed because it is fewer latency compared with the latency of the FIR filter.

Fig. 18 shows the SNDR versus input frequency with and without calibration in two-channel TI-ADC for $\Delta_{g0} = \Delta_{g1} = \Delta_{t0} = 0$ and $\Delta_{t1} = 0.01$. The parameters of the filter are applied in Table I. The proposed calibration gives 0.5 dB SNDR degradation for input frequency up to 0.45 F_s. The more filter taps can offer more wide bandwidth.

Fig. 19 shows the SNDR versus the sample-time mismatch with and without calibration in the two-channel TI-ADC. The input signal is sinusoidal at $\omega = 0.45 f_s$. The weight ω_{t1} is applied by the ideal value $(\Delta_{t0} - \Delta_{t1})/2$ as shown in (10). The proposed calibration gives 0.5 dB SNDR degradation for the mismatch up to 0.08. To increase SNDR for more large mismatch, more taps are needed to accurately approximate the exact transfer function in (7).

VI. Conclusion

The area-efficient all-digital background calibration technique in the TI-ADC has been presented. The proposed technique using the pseudo aliasing signals instead of the bank of adaptive filters which are conventionally utilized can greatly reduce the hardware of the mismatch correction. The pseudo aliasing signals are generated by the Hadamard transform and the fixed FIR filter and subtracted from the ADC output. In case of the two-channel 10-bit TI-ADC, the proposed technique reduces the requirement for the signal word length of the FIR filter by about 50% without the LUT compared with the conventional technique. In addition, the proposed technique requires only one FIR filter compared with the bank of adaptive filters which requires (M-1) FIR filters in the M-channel TI-ADC.

References

[1] W. C. Black, Jr. and D. A. Hodges, "Time interleaved converter arrays," *IEEE J. Solid-State Circuits*, vol. SC-15, pp. 1022–1029, Dec. 1980.

[2] N. Kurosawa, H. Kobayashi, L. Maruyama, H. Sugawara, and K. Kobayashi, "Explicit analysis of channel mismatch effects in time-interleaved ADC systems," *IEEE Trans. Circuits Syst. I, Fundam. Theory Appl.*, vol. 48, no. 3, Mar. 2001.

[3] M. Il-Chammas and B. Murmann, "General analysis on the impact of phase-skew in time-interleaved ADCs," *IEEE Trans. Circuits Syst. I, Reg. Papers*, vol. 56, no. 5, Mar. 2009.

[4] A. Haftbaradaran and K. W. Martin, "A background sample-time error calibration technique using random data for wide-band high-resolution time-interleaved ADCs," *IEEE Trans. Circuits Syst. II, Exp. Briefs*, vol. 55, no. 3, Mar. 2008.

[5] C.-Y. Wang and J.-T. Wu, "A multiphase timing-skew calibration technique using zero-crossing detection," *IEEE Trans. Circuits Syst. I*, vol. 56, no. 6, pp. 1102–1114, Jun. 2009.

[6] C.-C. Huang, C.-Y. Wang, and J.-T. Wu, "A CMOS 6-bit 16-GS/s time-interleaved ADC using digital background calibration techniques," *IEEE J. Solid-State Circuits*, vol. 46, no. 4, Apr. 2011.

[7] M. El-Chammas and B. Murmann, "A 12 GS/s 81-mW 5-bit time-interleaved flash ADC with background timing skew calibration," *IEEE J. Solid-State Circuits*, vol. 46, no. 4, pp. 838–847, Apr. 2011.

[8] S. M. Jamal, D. Fu, M. P. Singh, P. J. Hurst, and S. H. Lewis, "Calibration of sample-time error in a two-channel time-interleaved analog-to-digital converter," *IEEE Trans. Circuits Syst. I, Fundam. Theory Appl.*, vol. 51, no. 1, pp. 130–139, Jan. 2004.

[9] S. Huang and B. C. Levy, "Blind calibration of timing offsets for four-channel time-interleaved ADCs," *IEEE Trans. Circuits Syst. I, Reg. Papers*, vol. 54, no. 4, pp. 863–876, Jun. 2007.

[10] J. Elbornsson, F. Gustafsson, and J.-E. Eklund, "Blind equalization of time errors in a time-interleaved ADC system," *IEEE Trans. Signal Process.*, vol. 53, no. 4, pp. 1413–1424, Apl. 2005.

[11] T.-H. Tsai, P. J. Hurst, and S. H. Lewis, "Correction of mismatches in a time-interleaved analog-to-digital converter in an adaptively equalized digital communication receiver," *IEEE Trans. Circuits Syst. I*, vol. 56, no. 2, pp. 307–319, Jun. 2009.

[12] C. H. Law, P. J. Hurst, and S. H. Lewis, "A four-channel time-interleaved ADC with digital calibration of interchannel timing and memory errors," *IEEE J. Solid-State Circuits*, vol. 45, no. 10, pp. 2091–2103, Oct. 2010.

[13] S. M. Jamal, D. Fu, N. C.-J. Chang, P. J. Hurst, and S. H. Lewis, "A 10-b 120-Msample/s time-interleaved analog-to-digital converter with digital background calabration," *IEEE J. Solid-State Circuits*, vol. 37, no. 12, pp. 1618–1627, Dec. 2002.

[14] M. L. Honig and D. G. Messerschmitt, *Adaptive Filters*. Boston, MA, USA: Kluwer, 1984.

[15] V. Divi and G. W. Wornell, "Blind calibration of timing skew in time-interleaved analog-to-digital converters," *IEEE J. Sel. Topics Signal Process.*, vol. 3, no. 3, pp. 509–522, Jun. 2009.

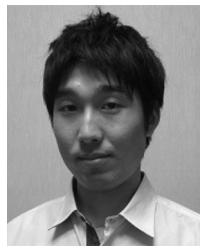

Junya Matsuno received the B.E. and M.E. degrees in electrical engineering from Tokyo University of Science, Chiba, Japan, in 2006 and 2008, respectively.

He joined the Corporate Research & Development Center, Toshiba Corp., Kawasaki, Japan, in 2008. Since then, he has been engaged in the research and development of wireless communication circuits. His current interests are mixed-signal processing and mixed-signal circuit design.

Takafumi Yamaji (M'98–SM'08) received the B.E., M.E., and Dr.Eng. degrees from Kyushu University, Fukuoka, Japan, in 1988, 1990, and 2004, respectively.

In 1990, he joined the Corporate Research & Development Center, Toshiba Corp., Kawasaki, Japan, where he was engaged in the research and development of analog integrated circuits for wireless communications. His research interests include mixed-signal processing and mixed-signal circuit design. He is currently the Chief Specialist of the Analog Device Design Department, Toshiba Corporation Semiconductor and Storage Products Company.

Masanori Furuta received the B.E. and M.E. degrees in information and computer sciences from Toyohashi University of Technology, Toyohashi, Japan, in 1998 and 2000, respectively, and the Ph.D. degree from Shizuoka University, Hamamatsu, Japan, in 2004.

From 2004 to 2007, he was a Research Associate with the Research Institute of Electronics, Shizuoka University. In 2007, he joined the Corporate Research and Development Center, Toshiba Corporation, Kawasaki, Japan. Since then, he has been engaged in the research and development of wireless communication circuits. His research interest is in the area of high-speed low-power A/D converter

Tetsuro Itakura (M'04) received the B.E. degree from Tokyo University of Agriculture and Technology, Tokyo, Japan, in 1981, the M.S. degree from Stanford University, Stanford, CA, in 1989, and the Dr.Eng. degree from Tokyo Institute of Technology, Tokyo, Japan, in 2003.

In 1981, he joined Toshiba Corp., Kawasaki, where he is with the Wireless System Laboratory, Corporate Research and Development Center. He has been engaged in the research and development of analog integrated circuits for telecommunications and for LCD driver ICs. His current interests are analog LSI design and signal processing.